Energy Conversion and Management 132 (2017) 438–451

Contents lists available at ScienceDirect

Energy Conversion and Management

journal homepage: www.elsevier.com/locate/enconman

Optimal control of conventional hydropower plant retrofitted with a cascaded pumpback system powered by an on-site hydrokinetic system

Fhazhil Wamalwa [a,*], Sam Sichilalu [a,b], Xiaohua Xia [a]

[a] Centre of New Energy Systems, Department of Electrical, Electronic and Computer Engineering, University of Pretoria, Pretoria 0002, South Africa
[b] Mosi-O-Tunya University of Science and Technology, Lusaka, Zambia

ARTICLE INFO

Article history:
Received 2 August 2016
Received in revised form 27 October 2016
Accepted 20 November 2016

Keywords:
Hydrokinetic generator
Cascaded-pumping
Pumpback operation
Hydropower
Hydraulic head
Optimal pumping strategy

ABSTRACT

This paper presents an optimal control strategy for a hydropower plant retrofitted with a hydrokinetic-powered cascaded pumpback system in dry season. Pumpback operation aims at recycling a part of the down-stream discharge back to the main dam to maintain a high water level to optimise the energy value of the available water. The problem is formulated as a multi-objective optimisation problem to simultaneously minimise the grid pumping energy demand, minimise the wear and tear associated with the switching frequency of the pumps, maximise the restoration of the volume of the dam through pumpback operation and maximise the use of on-site generated hydrokinetic power for pumping operation. The performance of the proposed cascaded model is compared with the classical single pump pumped storage model. Simulation results based on a practical case study shows that the cascaded pumpback model can reduce the pumping energy demand by up to 48.18% and increase the energy yield of the resultant system by up to 47.10% in dry season.

1. Introduction

Coping with the intermittent nature of hydropower generation is one of the main challenges faced by hydropower system operators. In the rainy season, the system operators are faced with a deluge of floods leading to excess power generation and spillage. The situation reverses in dry seasons with low in-stream flows where plant operators are compelled to curtail generation due to low water levels in the dams. The effects of this fluctuating nature of hydropower is more pronounced in predominantly hydropower systems in drought prone regions such as Southern Africa. Prolonged droughts experienced in the region in recent years have resulted in acute power shortages in many countries with Tanzania, Zimbabwe and Zambia worst affected because of their high reliance on hydropower.[1] The projected decrease in rainfall in Southern Africa underscores that the problem will become more pronounced [1–3]. This problem underscores the need to re-model the existing hydropower plants in the region to maximise the economic value of the available water. To this end, substantive researches on optimal control of hydropower systems have been accomplished in the current literature [4,5]. The main research focus is optimal planning and water resource allocation [6,7], optimal storage and scheduling of hydropower generators [8–11]. Optimal control of pumped storage (PS) systems in deregulated energy markets has also been studied extensively in the current literature [12–15]. In this case, the cheap-to-buy off-peak energy is used for pumping operation and later recovered and sold at peak prices to generate profits [13].

In systems with big disparities between peak and off-peak power demand, pumpback operation during off-peak hours to maintain a high reservoir water level for peak generation has been proposed by some researchers [16,17]. In [16], a pumpback operation to optimise energy yield of the plant over a 12-month control period with seasonal changes in instream flows as a sources of uncertainty is proposed. However, the author does not consider minimisation of pumping energy resulting in high pumping energy demand over the control period. In [17], a pumpback retrofit is proposed for a high head application to maximise the energy output and revenue of a hydropower plant in a market with deterministic time-varying energy prices over a 24-h control horizon with a constant in-stream flow. In this case, the high head losses associated with a single high lift pump has the potential to degrade the economic viability of the model. For instance, the model in [17] is proposed by the authors as effective for application to the 150 m head Eugenia Fall hydropower plant in Ontario. Pumping losses associated with such a high head can derail the economic viability of the model.

* Corresponding author.
E-mail addresses: Fhazhil.Wamalwa@up.ac.za, Fazil.wamalwa@gmail.com (F. Wamalwa).

[1] mg.co.za/article/2016-01-14-droughts-devastating-ripple-effect.

http://dx.doi.org/10.1016/j.enconman.2016.11.049
0196-8904/

Nomenclature

$n_{h,t}$	a control variable denoting the number of hydrokinetic generators
u_1, u_2	state of switches for the pumps
$P_{h,nom}$	the rated power output of a single hydrokinetic generator (MW)
$P_{h,t}$	hydrokinetic generator power output (MW)
$P_{hg,t}$	excess hydrokinetic power exported to the grid (MW)
$P_{hk,t}$	hydrokinetic power supplied to meet the pumping power demand (MW)
$P_{K,t}$	total pumping power demand of the pumpback system (MW)
$P_{K1,t}$	power demand by pump K1 (MW)
$P_{K2,t}$	power demand by pump K2 (MW)
$P_{g,t}$	hydroelectric plant power output (MW)
$H_{o,t}$	the hydraulic head of the dam (m)
$Q_{o,t}$	turbine flow rate of the dam via the penstock (m^3/s)
$P_{gk,t}$	pumping power demand imported from the grid (MW)
$h_{u,t}$	depth of the main dam (m)
$h_{r,t}$	depth of the intermediate reservoir (m)
η_e	the combined efficiency of the hydro turbine and the generator
P_g^{min}, P_g^{max}	minimum and maximum power output of a hydroelectric plant (MW)
Q_{in}	upper reservoir in-stream flow rate (m^3/s)
Q_1, Q_2	discharge rate of pumps K1 and K2 respectively (m^3/s)
t_s and k	sampling period (h) and k_{th} sampling interval
A_u	base area of the upper reservoir (m^2)
h_u^{min}, h_u^{min}	minimum and maximum water levels in the upper (dam) reservoir (m)
A_r	base area of intermediate reservoir (m^2)
h_r^{min}, h_r^{min}	minimum and maximum water levels in the intermediate reservoir (m)
H_1, H_2	net head of pump K1 and K2 respectively (m) respectively
η_{k1}, η_{k2}	efficiency of pumps K1 and K2 respectively
P_K^{min}, P_K^{min}	minimum and maximum pumping power demand (MW)
η_t, η_g	the hydrokinetic turbine and generator efficiency
C_p	coefficient of performance of the hydrokinetic turbine
A_t	cross sectional area of the hydrokinetic turbine (m^2)
v	river current velocity (m/s)
P_h^{min}, P_h^{min}	minimum and maximum hydrokinetic generator power output (MW)
N	total number of sampling intervals
J	the objective function
$P_{ld,t}$	total grid load demand (MW)
Res_{opt}	the optimal change in the intermediate reservoir water level due to pumping operation (m)
H_{K1}	change in the intermediate reservoir water level due to K1 operation (m)
H_{K2}	change in the intermediate reservoir water level due to K2 operation (m)
H_{Qo}	change in the main dam water level due to Q_o (m)
H_{inflow}	change in the main dam water level due to the combined state inflows (m)
H_{opt}	optimal change in the main dam water level due to the combined state inflows and outflows (m)
E_g	total energy produced by the hydro-turbine generator over the 24-h control period (MW h)
E_h	total energy produced by the hydrokinetic system over the 24-h control period (MW h)
E_{hk}	total hydro-turbine energy consumed by pumping system over the 24-h control period (MW h)
E_{hg}	total hydrokinetic energy exported to the grid over the 24-h control period (MW h)
E_{gk}	total grid energy supplied to the pumping system over the 24-h control period (MW h)
E_{opt}	total optimal energy output of the system over the 24-h control period (MW h)

In this paper, unlike in the cited works, we seek to simultaneously minimise the pumping energy demand and the wear and tear associated with the switching frequency of the pumping system. We further propose an on-site hydrokinetic energy conversion (HEC) system for powering the pumpback system instead of full reliance on grid power. To minimise pumping power demand for high head applications, we further propose a cascaded pumpback model with two pumps inter-staged with an intermediate reservoir to reduce the hydraulic head to be bridged by a single high power high lift pump. A cascaded model reduces the overall pumping problem into a multi-pump operation problem which can be solved to minimise the pumping power demand of the resultant system. Defining a pump switch as a state transition of a pump from off to on state [18], the problem of optimal switching control of a pumping system to minimise the pumping energy demand has been solved in [19,20]. Since pumping energy demand over a given control period is proportional to the number of switches or the cumulative operating hours, a pumping optimisation problem can be formulated to minimise the number of pump switches [21] as well as the cumulative number of operating hours [18]. The main contribution of this work include: (1) The use of alternative hydrokinetic (HK) energy for pumping operation, (2) cascading pumpback operation to minimise pumping power and energy demand for high head applications and (3) minimisation of the wear and tear costs of the pumps by minimising the number of switches of each of the pumps. This paper is organised as follows: Sections 2 and 3 present the mathematical formulation and discrete time modelling of the system respectively. Section 4 presents the simulation results and discussion while the last part, Section 6, concludes the paper.

2. Mathematical model formulation

2.1. Schematic model layout

Fig. 1 shows the schematic layout of the proposed hydropower model with a cascaded pumpback retrofit. In the figure, $H_{o,t}(m)$ is the system head while $h_{u,t}(m)$ is the height (depth) of water in the dam at any given time t. The system comprises the conventional hydropower system, the HEC system and the cascaded pumpback system. The conventional hydropower system comprises the main dam and the hydro-turbine generator in the power house. The HEC system comprises n_h hydrokinetic generators installed in the tail-race of the power plant to harness a part of the kinetic energy of free-flowing water to power the pumpback system. The pumpback system comprises pumps $K1$ and $K2$ powered through their respective switches u_1 and u_2 and the intermediate reservoir R.

In the proposed model, the pumping power demand will be met primarily by the on-site generated HK power. In cases when the on-site generated HK power is more than the pumping power demand, the surplus will be exported to the grid. Conversely, when the HK power output is less than the pumping power demand, the

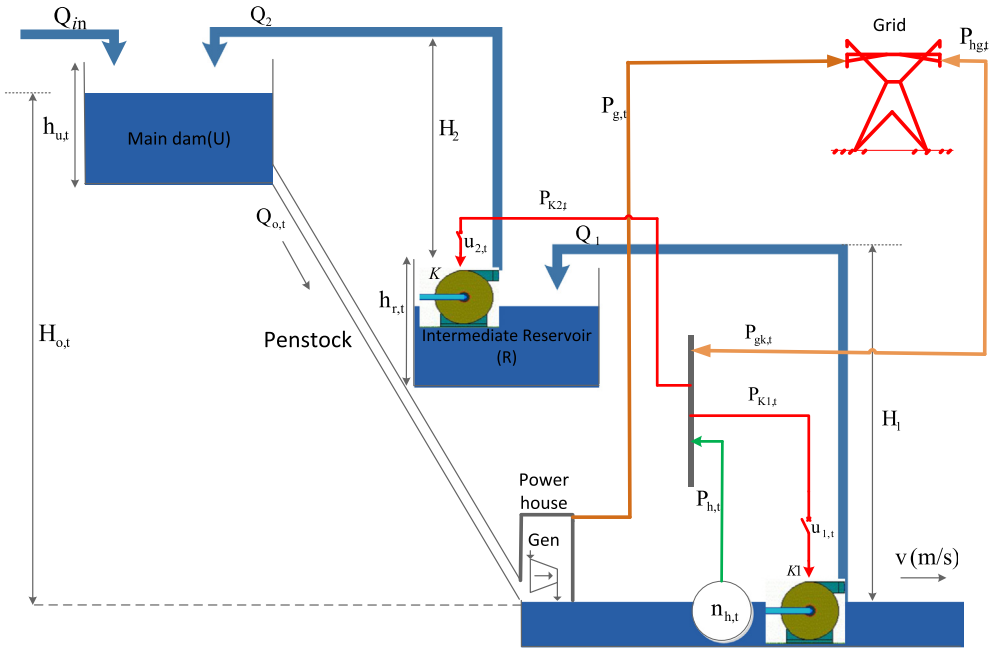

Fig. 1. Schematic layout of the hydropower system with cascaded HK-powered pumpback system.

deficit will be offset by grid power import, $P_{gk,t}$. In Fig. 1, $P_{g,t}$ and $P_{h,t}$ are respectively, the hydro-turbine generator and the HK power output. The fraction of HK power supplied to meet the pump load is denoted by $P_{hk,t}$ while $P_{hg,t}$ is the excess on-site generated HK power exported to the grid. The notations $P_{K1,t}$ and $P_{K2,t}$ are respectively, the pumping power demand for pumps $K1$ and $K2$. The quantities Q_{in}, $Q_{o,t}$, Q_1 and Q_2 are respectively, the constant in-stream flow rate, the turbine discharge rate and the flow rates of pumps $K1$ and $K2$ expressed in m^3/s. The speed of water down-stream, v (m/s), is assumed to be constant over the 24-h control period in this paper. It is also assumed that down-stream river flow is un-regulated and the dam is a single purpose dam for hydropower generation only. In this model, the control variables include $Q_{o,t}$, $n_{h,t}$, $P_{gk,t}$, $P_{hk,t}$, $P_{hg,t}$ and the state of the pump switches, $u_{1,t}$ and $u_{2,t}$. The water level in the main dam, $h_{u,t}$, and the level in the intermediate reservoir, $h_{r,t}$, form the state variables of the system.

2.2. Sub models

2.2.1. Conventional hydropower model

Given the density of water, $\rho = 1000\ kg/m^3$ and gravitational acceleration, $g = 9.81\ m/s^2$, theoretical power output of a hydro-turbine generator, $P_{g,t}$ (MW), can be expressed as a non-linear function of the net head of the system, $H_{o,t}$ (m), and the turbine flow rate, $Q_{o,t}$ (m^3/s), as follows [22]:

$$P_{g,t} = 9.81\eta_e H_{o,t} Q_{o,t} \times 10^{-3}, \quad 0 \leqslant Q_{o,t} \leqslant A_p\sqrt{2gH_o^{max}} \tag{1}$$

where η_e, $A_p(m^2)$ and H_o^{max} (m) are respectively, the overall efficiency of the hydro-turbine generator, the cross-sectional area of the penstock and the maximum head of the system.

If a cylindrical model with a base area, $A_u(m^2)$, is assumed for the main dam and the precipitation to and evaporation losses from the water surface is neglected for a short scheduling period, the water mass balance of the dam can be expressed by a first order differential equation as follows [16]:

$$h_{u,t+1} = h_{u,t} + \frac{t_s}{A_u}\left[Q_{in} + u_{2,t}Q_2 - Q_{o,t}\right], \tag{2}$$

where $h_{u,t}$ and $h_{u,t+1}$ are respectively, the dam water level at the end of time t and the next time period, $t+1$. The notation $u_{2,t}$ is a binary variable [0,1] denoting the on/off state of the switch of pump $K2$ while t_s is the sampling time. For optimal operation, the water level in the dam must not exceed its dimensions and must not fall below the minimum operational limit. Therefore, the dam level is restricted to lie within $h_{u,t} \in [h_u^{min}, h_u^{max}]$ where h_u^{min} and h_u^{max} are respectively, the minimum and maximum operational bounds of the dam.

Similarly, if we assume a cylindrical model with a base area, $A_r(m^2)$ and zero evaporation and precipitation effects for a short scheduling period, the water mass balance of the intermediate reservoir can be expressed in terms of reservoir height as follows:

$$h_{r,t+1} = h_{r,t} + \frac{t_s}{A_u}\left[u_{1,t}Q_1 - u_{2,t}Q_2\right], \tag{3}$$

where $h_{r,t}$ (m) and $h_{r,t+1}$ (m) are respectively, the height of water in the reservoir at the end of time t and at the end of the next time phase, $t+1$. Similarly, the water level in the intermediate reservoir at any given time is constrained to lie within $h_{r,t} \in [h_r^{min}, h_r^{max}]$ where h_r^{min} and h_r^{max} are respectively, the minimum and the maximum operational bounds of the intermediate reservoir.

2.3. Cascaded pumping model

The pumpback operation conserves water by recycling a part of the down-stream discharge back to the main dam to maintain a high level for optimal hydropower generation; the amount of water discharged for each unit of hydropower generated increases with a decrease in the level of water in the dam. The proposed model employs constant speed pumps assumed to work at their full rated capacity and controlled by on/off switches. Therefore, the pumping power demand of each pump depends only on the status of the on/off switches expressed as follows [23]:

$$P_{Ki,t} = \frac{9.81 H_i Q_i u_{i,t}}{\eta_{ki}} \times 10^{-3}, \quad i = 1, 2, \tag{4}$$

where $P_{Ki,t}$ (MW), H_i, Q_i and u_i are respectively, the power demand, the hydraulic head, the flow rate and the control switch of pump *Ki* at time *t*. The coefficient η_{ki} denotes the combined efficiency of pump *Ki* and its drive motor. In the proposed model, the pumping power demand is met primarily by the power flow from the HEC system, $P_{hk,t}$. In cases when the on-site generated power is less than the pumping power demand, grid power, $P_{gk,t}$, will be imported to off-set the deficit. Therefore, the power balance of the pumpback system can be expressed as follows:

$$P_{hk,t} + P_{gk,t} = P_{K1,t} u_{1,t} + P_{K2,t} u_{2,t}. \tag{5}$$

2.3.1. HEC system

Unlike the conventional hydro turbine generator that requires a water head, a HK generator is designed to extract the kinetic energy of the run-off water at low to zero hydraulic head and convert it into electrical energy [24]. The operation principle of a HK turbine is similar to that of a wind turbine and thus, the power output of a HEC system can be expressed by Eq. (6) adopted from [25].

$$P_{h,t} = \frac{1}{2} C_p \eta_t \eta_g A_t \rho v^3 \times 10^{-6}, \tag{6}$$

where C_p, $A_t(m^2)$ and v(m/s) are respectively, the coefficient of performance of the HEC system limited by Betz law [26], the area swept by the HK turbine rotor and the after-bay speed of water. The coefficients η_t and η_g are respectively, the efficiencies of the HK turbine and the generator while ρ is the density of water expressed in kg/m^3. In general, the power output of the HEC system,$P_{h,t}$ (MW), depends on the number of HK generators in parallel operation, $n_{h,t}$, and the nominal power rating of each of the HK generators, $P_{h,nom}$, expressed by Eq. (7).

$$P_{h,t} = n_{h,t} P_{h,nom}. \tag{7}$$

Therefore, the power balance of the HEC system is expressed as follows:

$$P_{h,t} = P_{hk,t} + P_{hg,t}, \tag{8}$$

3. Discrete model formulation of the system

The state dynamics of the dam Eq. (2) can be re-expressed in discrete time domain by a first order differential equation as follows:

$$h_{u,k+1} = h_{u,k} + \frac{t_s}{A_u}\left[Q_{in} + u_{2,k} Q_2 - Q_{o,k}\right], \tag{9}$$

which can be expressed iteratively as follows:

$$\begin{aligned}
&k=0; \quad h_{u,1} = h_{u,0} + \frac{Q_{in} t_s}{A_u} + \frac{u_{2,0} Q_2 t_s}{A_u} - \frac{Q_{o,0} t_s}{A_u},\\
&k=1; \quad h_{u,2} = h_{u,1} + \frac{Q_{in} t_s}{A_u} + \frac{u_{2,1} Q_2 t_s}{A_u} - \frac{Q_{o,1} t_s}{A_u},\\
&k=2; \quad h_{u,3} = h_{u,2} + \frac{Q_{in} t_s}{A_u} + \frac{u_{2,2} Q_2 t_s}{A_u} - \frac{Q_{o,2} t_s}{A_u},\\
&\vdots\\
&h_{u,k} = h_{u,0} + \frac{t_s Q_{in}}{A_u} + \frac{t_s Q_2}{A_u}\sum_{j=1}^{k} u_{2,j} - \frac{t_s}{A_u}\sum_{j=1}^{k} Q_{o,j}, \quad (1 \leqslant j \leqslant k),
\end{aligned} \tag{10}$$

where k is the sampling interval and $h_{u,0}$ is the initial water level in the dam at time $k = 0$. Therefore, the water level constraint of the main dam can be expressed in discrete time domain as follows:

$$h_u^{min} \leqslant h_{u,0} + \frac{t_s Q_{in}}{A_u} + \frac{t_s Q_2}{A_u}\sum_{j=1}^{k} u_{2,j} - \frac{t_s}{A_u}\sum_{j=1}^{k} Q_{o,j} \leqslant h_u^{max}. \tag{11}$$

Similarly, the intermediate reservoir water mass balance Eq. (3) can be re-expressed in discretised form as follows:

$$\begin{aligned}
&h_{r,k+1} = h_{r,k} + \frac{t_s}{A_r}\left[u_{1,k} Q_1 - u_{2,k} Q_2\right],\\
&k=0; \quad h_{r,1} = h_{r,0} + \frac{t_s}{A_r}[u_{1,0} Q_1 - u_{2,0} Q_2],\\
&k=1; \quad h_{r,2} = h_{r,1} + \frac{t_s}{A_r}[u_{1,1} Q_1 - u_{2,1} Q_2],\\
&k=2; \quad h_{r,3} = h_{r,2} + \frac{t_s}{A_r}[u_{1,2} Q_1 - u_{2,2} Q_2],\\
&\vdots\\
&h_{r,k} = h_{r,0} + \frac{t_s Q_1}{A_r}\sum_{j=1}^{k} u_{1,j} - \frac{t_s Q_2}{A_r}\sum_{j=1}^{k} u_{2,j}, \quad (1 \leqslant j \leqslant k),
\end{aligned} \tag{12}$$

where $h_{r,0}$ is the water level in the intermediate reservoir when $k = 0$. The constraint of water level in the intermediate reservoir is expressed in discrete form as follows:

$$h_r^{min} \leqslant h_{r,0} + \frac{t_s Q_1}{A_r}\sum_{j=1}^{k} u_{1,j} - \frac{t_s Q_2}{A_r}\sum_{j=1}^{k} u_{2,j} \leqslant h_r^{max}. \tag{13}$$

3.1. Objective function

The problem is formulated as a multi-objective optimisation problem given by Eq. (14). The first performance index, $t_s\sum_{k=1}^{N} P_{gk,k}$ minimises the grid pumping energy demand. The second part, $\sum_{k=1}^{N}(s_{1,k} + s_{2,k})$ minimises the switching frequency of the two pumps, K1 and K2, to reduce wear-and-tear. The third objective, $t_s\sum_{k=1}^{N} Q_2 u_{2,k}$ maximises the restoration of the water volume in the main dam through pumpback operation while the fourth objective, $t_s\sum_{k=1}^{N} P_{hk,k}$ maximises the use of hydrokinetic energy to power the pumpback system. Finally, the overall performance index is written as follows:

$$J = w_1 t_s \sum_{k=1}^{N} P_{gk,k} + w_2 t_s \sum_{k=1}^{N}(s_{1,k} + s_{2,k}) - w_3 t_s \sum_{k=1}^{N} Q_2 u_{2,k} - w_4 t_s \sum_{k=1}^{N} P_{hk,k}, \tag{14}$$

The control horizon is 24 h with a sampling time, $t_s = 0.25h$. $k = 1, \ldots, N$ is sampling interval and N is the total number of intervals.

In general, the maintenance cost of a pump relates to wear and tear costs associated with the number of switching times [27]. Therefore, minimisation of the switching times of a pump reduces its associated wear and tear costs. In this paper, the Pretorian method used in [27] is used to minimise the switching frequency of the pumps. This method introduces an auxiliary variable, s_k represented by a value of 1 whenever a transition from off to on state of the pump occurs. Minimising the state transitions of the auxiliary variable, s_k reduces the switching frequency of the pump by augmenting the adjacent on/off switches and consequently reducing the overall number of switches of each of the pumps over the 24 h control horizon.

The objective function Eq. (14) is solved subject to the following constraints:

$$h_u^{min} \leqslant h_{u,0} + \frac{t_s Q_{in}}{A_u} + \frac{t_s Q_2}{A_u}\sum_{j=1}^{k} u_{2,j} - \frac{t_s}{A_u}\sum_{j=1}^{k} Q_{o,j} \leqslant h_u^{max}, \tag{15}$$

$$h_r^{min} \leqslant h_{r,0} + \frac{t_s Q_1}{A_r}\sum_{j=1}^{k} u_{1,j} - \frac{t_s Q_2}{A_r}\sum_{j=1}^{k} u_{2,j} \leqslant h_r^{max}, \tag{16}$$

$$P_{g,k} + P_{hg,k} = P_{ld,k}, \tag{17}$$

$$P_{h,k} = P_{hk,k} + P_{hg,k}, \tag{18}$$

$$P_{hk,k} + P_{gk,k} = u_{1,k}P_{K1} + u_{2,k}P_{K2}, \tag{19}$$

$$P_g^{min} \leqslant P_{g,k} \leqslant P_g^{max}, \quad 0 \leqslant Q_{o,k} \leqslant A_p\sqrt{2gH_o^{max}} \tag{20}$$

$$P_h^{min} \leqslant P_{h,k} \leqslant P_h^{max} \tag{21}$$

$$P_{hg}^{min} \leqslant P_{hg,k} \leqslant P_{hg}^{max} \tag{22}$$

$$P_{hk}^{min} \leqslant P_{hk,k} \leqslant P_{hk}^{max} \tag{23}$$

$$P_{gk}^{min} \leqslant P_{gk,k} \leqslant P_{gk}^{max} \tag{24}$$

$$u_{i,k} - s_{i,k} \leqslant 0, i = 1,2 \quad s_{i,k} \in [0,1] \tag{25}$$

$$u_{i,k} - u_{i,k-1} - s_{i,k} \leqslant 0, \quad i = 1,2 \tag{26}$$

$$u_{i,k} \in [0,1], \quad i = 1,2, \quad (1 \leqslant k \leqslant N), \tag{27}$$

where $\sum_{j=1}^{4} w_j = 1$ is the weighting factors that determine the relative importance of each of the objective vectors. Inequalities (15) and (16) are respectively, the state constraints of the dam and the intermediate reservoir bounded by their respective minimum and maximum allowable limits. The equalities (17) and (18) are the grid and the HK power balances respectively. Equality (17) shows that the power supplied to the grid is the sum of the hydro turbine generator output and the excess HK power. Equality (19) shows that the total power demand by the pumpback system is the sum of the HK power supplied to the pumps and the supplementary grid power import. Inequalities (20)–(24) are respectively, the control variable bounds for: the hydro-turbine generator power output which depends on the turbine flow rate bounds, the total HK power output, the surplus HK power exported to the grid, the HK power supplied to meet the pumping power demand and the supplementary grid power imported to offset pumping power deficit. The inequality (25) initialises the auxiliary variable $s_{i,k}$ as the initial status of $u_{i,k}$ while the inequality (26) favours the control with less switching frequency. These auxiliary constraints allow the objective function (14) to simultaneously minimise the grid pumping energy demand, minimise the wear and tear costs by minimising the number of on/off switching of the pumpback system, maximise restoration of the volume of the main dam through pumpback operation and maximise the use of HK energy for pumping operation. Eq. (27) is a binary control variable constraint for the switches, u_1 and u_2, which control pumps $K1$ and $K2$ respectively.

3.2. Algorithm formulation and implementation in MATLAB

The proposed model yields a constrained mixed integer nonlinear problem solvable by the *OPTI toolbox* SCIP algorithm in MATLAB. The control variables are as follows: binary variables, $u_{1,k}$ and $u_{2,k}$, real number variables; $Q_{o,k}, P_{hk,k}, P_{hg,k}$ and $P_{gk,k}$, an integer variable, $n_{h,k}$, and the auxiliary variable, $s_{i,k}, i = 1,2$. The objective function Eq. (14) is expressed in canonical form by Eq. (28).

$$f^T\mathbf{X} \tag{28}$$

subject to

$$\begin{cases} \mathbf{AX} \leqslant \mathbf{b} \\ \mathbf{A_{eq}X} = \mathbf{b_{eq}} \\ \mathbf{L_B} \leqslant \mathbf{X} \leqslant \mathbf{L_B}. \end{cases} \tag{29}$$

where $\mathbf{AX} \leqslant \mathbf{b}$ denotes the inequality constraints, $\mathbf{A_{eq}X} = \mathbf{b_{eq}}$ the equality constraints and $\mathbf{L_B} \leqslant \mathbf{X} \leqslant \mathbf{L_B}$ denotes the lower and the upper bounds of the control variables.

The vector $\mathbf{X}$ contains all the control variables of the model expressed by Eq. (30).

$$\mathbf{X} = \left[u_{1,1\ldots N},\ u_{2,1\ldots N},\ n_{h,1\ldots N},\ Q_{o,1\ldots N},\ P_{hk,1\ldots N},\ P_{gk,1\ldots N},\ P_{hg,1\ldots N},\ s_{1,1\ldots N},\ s_{2,1\ldots N}\right]'_{9N\times 1}. \tag{30}$$

From the objective function Eq. (14):

$$f^T = \left[0_{1\ldots N},\ -w_3Q_{2,1\ldots N},\ 0_{1\ldots N},\ 0_{1\ldots N},\ w_{1,1\ldots N},\ w_{1,1\ldots N},\ 0_{1\ldots N}, w_{2,1\ldots N}, w_{2,1\ldots N}\right]_{1\times 9N}. \tag{31}$$

The lower and the upper bounds of the control variables are expressed by Eqs. (32) and (33).

Lower bounds

$$lb^T = \left[0_{1\ldots N},\ 0_{1\ldots N},\ 0_{1\ldots N},\ 0_{1\ldots N},\ 0_{1\ldots N},\ 0_{1\ldots N},\ 0_{1\ldots N}, 0_{1\ldots N}, 0_{1\ldots N}\right]_{9N\times 1}. \tag{32}$$

Upper bounds

$$ub^T = \left[1_{1\ldots N},\ 1_{1\ldots N},\ 32_{1\ldots N},\ 45_{1\ldots N},\ \sum_{j=1}^{2} P_{Kj,1\ldots N},\ \sum_{j=1}^{2} P_{Kj,1\ldots N},\ n_h P_{h,1\ldots N},\ 1_{1\ldots N},\ 1_{1\ldots N}\right]_{1\times 9N}. \tag{33}$$

The detailed formulation of the inequality and equality constraints of the problem are attached to Appendix A.

3.3. Case study

The case study is based on Pangani fall hydropower plant (HPP), one of the three HPPs that form a cascade of the Pangani Hydropower system located on Pangani River in Tanzania. The first one is Nyumba ya mungu (NyM) plant, a 2×4 MW hydropower plant located at NyM dam which discharges into the 2×10.5 MW Hale HPP. From the Hale power plant, water flows into the Pangani fall dam that feeds the 2×34 MW Pangani fall HPP which drains into the Indian Ocean 64 km downstream. The Pangani hydropower system has a total installed capacity of 91.5 MW. However, the generation capacity drops to 30% during dry seasons due to low water levels in the dams; a situation which has worsened in recent years due to prolonged droughts[2] caused by the on-going climate change. Hydropower generation of the Pangani fall HPP has declined in the last 10 years [28] and reached the lowest point in 2014 with a production of 25 MW; a situation that threatened its shutdown.[3] In this work, we propose a pumpback retrofit to recycle a part of the after-bay water back to the main dam to maintain a high level in the dam to optimise its energy yield. We propose a cascaded pumpback system to minimise the pumping energy demand of the system through optimal scheduling and operation of the pumps. To validate the economic advantages of the proposed cascaded pumpback model over the classical single pump pumpback model, the performance of the hydropower plant is simulated over a control period of 24 h for each of the models. The simulation assumes a normal average day in dry and rainy seasons with a constant river discharge. However, in practice, the river discharge may vary if the system is modelled for a longer horizon such as for a month or a year depending on precipitation patterns of the region.

3.3.1. Pangani fall hydropower plant

Pangani fall HPP is fed by Pangani fall dam with a live capacity of 0.8×10^6 m^3. The reservoir has a maximum and minimum hydropower operating level by volume of 1.7×10^6 m^3 and

[2] http://www.iucn.org/dbtw-wpd/edocs/2007-002.pdf.

[3] http://www.theeastafrican.co.ke/news/Tanzania-to-switch-off-all-hydropower-stations/-/2558/2905900/-/ep5kq9/-/index.html.

Table 1
Salient features of Pangani fall hydropower plant.

Res-vol (m^3)	h_u^{max} (masl)	h_u^{min} (masl)	H_o (masl)	P_g (rated) (MW)	Q_o^{max} (m^3/s)	Q_o^{min} (m^3/s)	Q_{in} (m^3/s)	η_e
1.4×10^6	177.50	176.00	170.00	68.00	45.00	9.00	12.50	0.93

Table 2
Design specifications of the intermediate reservoir.

Design shape	Design capacity m^3	Radius (m)	Design height (m)	h_r^{max} (m)	h_r^{min} (m)
Cylindrical	2.40×10^5	35.60	60.00	60.00	10.00

Table 3
Design specifications of the pumping system.

Q_1 (m^3/s)	Q_2 (m^3/s)	H_1 (m)	H_2 (m)	Head range (m)	Pressure (bar)	η_p
5.50	5.50	85.00	85.00	up to 110.00	up to 64.00	0.90

0.9×10^6 m^3 respectively. The plant is installed with 2×34 MW SAV340/110/14 generators with a nominal capacity of 2×40 MVA and a power factor of 0.85. The plant turbines' speed is 428 rpm (rpm) [29]. In this case study, an initial volume of 1.1×10^6 m^3 is assumed, which is a typical average capacity of Pangani fall dam in dry season. For ease of modelling and control of the available capacity, a cylindrical model with a base radius of 71.36 m which gives the dam model a design depth of 68.75 m. Table 1 shows the salient features of Pangani fall HPP with the height given in meters above sea level (masl) [29].

3.3.2. Intermediate reservoir parameters

The intermediate reservoir, *R*, proposed in this model is used to create an intermediate pumping stage for operation of pumps *K*1 and *K*2 in cascade as shown in Fig. 1. This reservoir is sized by rule of thumb to ensure 12-h continuous outward pumping by K2 without restorative inward pumping by K1 and 12-h inward pumping by K1 without outward pumping by K2. Since the two pumps K_1 and K_2 are sized equally, the maximum capacity of the intermediate reservoir can be approximated to $2.4 \times 10^5 m^3$ with a design radius of 35.60 m and a height of 60.0 m. Table 2 shows the design specifications of the intermediate reservoir.

3.3.3. Cascaded pumping system parameters

The pumps used in the case study are the SJT vertical turbine pumps from Sulzar Ltd with a performance range of up to 17.30 m^3/s, maximum head of 110 m and pressure of up to 64 bar.[4] Table 3 shows the specifications of the pumps used in the case study.

3.3.4. Hydrokinetic generator parameters

The hydrokinetic energy conversion system used in the case study comprise of the CC035A river-in-stream turbine models developed by the Clean Current Renewable Energy Systems Inc[5] and the flooded, permanent magnet generators. The CC035A turbine has a rotor diameter of 3.50 m and requires a minimum river depth of 7.00 m for effective deployment. The technical specifications of the HK turbines used in this paper are given in Table 4. η_t denotes the efficiency of the mechanical gear box of the turbine. However, the Betz limit, C_p is factored in the power output model given in Eq. (6).

The CC035A HK turbine model has a rated power output of 65 kW and a nominal revolution per minute (rpm) of 75. It operates optimally in a current speed range of 1.50–3.70 m/s. The hydrokinetic generator has a nominal output of 65 kW.

3.3.5. Uncertainty analysis of the demand load

There are several techniques used in sensitivity (uncertainty) analysis in a given model to determine its viability and reliability at design stage. In this paper we adopted the methodology used in [30] to ascertain the confidence level of the load demand in the case study. The random error (noise) in addition to the instrument's absolute uncertainty is introduced in the load demand which in this case is the recorded load profile of the hydropower plant referred to as the measured value. The true (accepted) values are then estimated from the measured (corrupted) values. The resulting difference between measured and true values is due to random errors. For analysis purposes, random errors are generated in MATLAB software with a distribution mean of 0 and standard deviation of 1 which is then multiplied by the absolute uncertainty of the watt-meter $\sigma_{m,meas} = \pm 0.01$; a value which is often given by the manufacturer of the demand measuring instrument.

$$Z_m = A_m + RAND_m * \sigma_{m,meas}. \tag{34}$$

where $Z_m, A_m, RAND_m$ and $\sigma_{m,meas}$ are respectively, the measured value of *m*th measurement, the true value, the random noise and the standard deviation of the *m*th measurement while $m = 1, \ldots, 24$ is the number of measurements. The Pangani fall hydropower load demand profile is analysed for sensitivity and the results are shown in Table 5. Further analysis is done to determine the relative uncertainty of each given measurement.

$$\text{Relative uncertainty } (\%) = \frac{\text{Absolute uncertainty}}{\text{Measured value}}. \tag{35}$$

In this case, the weakest link rule[6] is applied where the measurement with the largest relative uncertainty is picked from Table 5. In this case, the largest relative uncertainty is 0.022% which is used to determine the absolute uncertainty of the final objective function.

The simulation is performed for both measured and true values, A_m, to compare the confidence level of the results of the proposed

[4] https://www.sulzer.com/en/Products-and-Services/Pumps-and-Systems/Vertical-Pumps/Vertical-Wet-Pit-Pumps/SJT-Vertical-Turbine-Pumps.
[5] http://www.cleancurrent.com/river-turbines.
[6] http://www2.fiu.edu/dbrookes/ExperimentalUncertaintiesCalculus.pdfDateaccessed10.10.2016.

Table 4
Hydrokinetic turbine specifications.

Model	n_h	P_h (kW)	A_t (m^2)	V_{rated} (m/s)	η_t (%)	η_g (%)	ρ_w (kg/m^3)	C_p
CC035A	26.00	65.00	9.60	3.00	0.90	0.85	1000	0.45

Table 5
Uncertainty analysis of the Pangani fall HPP on load demand profile.

Measured values (MW)	Rand error	$\sigma_{m,meas}$	True values (MW)	Absolute uncertainty	Relative uncertainty (%)
50	0.534	0.01	49.995	(50 ± 0.01)	0.020
50	0.885	0.01	49.991	(50 ± 0.01)	0.020
50	0.899	0.01	49.991	(50 ± 0.01)	0.020
50	0.626	0.01	49.994	(50 ± 0.01)	0.020
60	0.138	0.01	59.999	(60 ± 0.01)	0.017
60	0.218	0.01	59.998	(60 ± 0.01)	0.017
60	0.182	0.01	59.998	(60 ± 0.01)	0.017
60	0.042	0.01	60.000	(60 ± 0.01)	0.017
60	0.107	0.01	59.999	(60 ± 0.01)	0.017
60	0.616	0.01	59.994	(60 ± 0.01)	0.017
60	0.940	0.01	59.991	(60 ± 0.01)	0.017
60	0.355	0.01	59.996	(60 ± 0.01)	0.017
65	0.411	0.01	64.996	(65 ± 0.01)	0.015
65	0.984	0.01	64.990	(65 ± 0.01)	0.015
65	0.946	0.01	64.991	(65 ± 0.01)	0.015
65	0.677	0.01	64.993	(65 ± 0.01)	0.015
45	0.988	0.01	44.990	(45 ± 0.01)	0.022
45	0.767	0.01	44.992	(45 ± 0.01)	0.022
45	0.337	0.01	44.997	(45 ± 0.01)	0.022
45	0.662	0.01	44.993	(45 ± 0.01)	0.022
45	0.244	0.01	44.998	(45 ± 0.01)	0.022
45	0.296	0.01	44.997	(45 ± 0.01)	0.022
45	0.680	0.01	44.993	(45 ± 0.01)	0.022
45	0.528	0.01	44.995	(45 ± 0.01)	0.022

model. The measured and true value simulation results are presented in Figs. 4 and 5 respectively in Section 4.3.

4. Simulation results and discussion

The optimal control is modelled for two scenarios. The first scenario simulates a typical day in a dry season when there is low river inflow, modelling a drought season case. The second scenario simulates the performance of the model on a typical day in the rainy season with high in-stream discharge. To validate, the performance advantages of the cascaded pump-back model, simulation for a single pump classical PS model is also carried out for the two scenarios. The comparison of the performance of the two models is presented in Section 5.

Scenario I

4.1. Optimal switching operation of the pumpback system

Fig. 2 shows the results of the optimal switching of the cascaded pumpback model and the resultant change in water level of the intermediate reservoir obtained for the case when $w_1 = w_2 = w_3 = w_4 = 0.25$. The minimum operation level of the intermediate reservoir is set at 10.00 m while the initial water level is set at 15.00 m. As a result, the OC switches on pump K1 between 00:00 and 11:00 to raise the water level of the intermediate reservoir before bringing in pump K2 for onward pumping to the main dam. As shown in Fig. 2, the OC switches off pump K1 at 11:00 and switches on K2 for the remainder of the control horizon to keep a

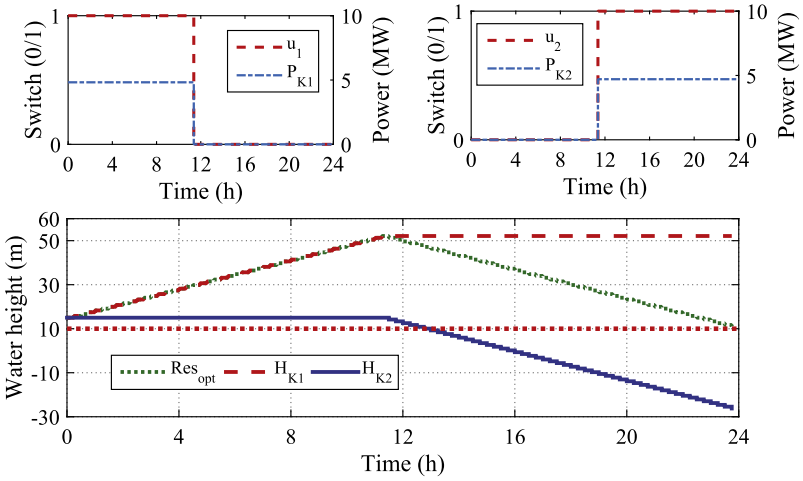

Fig. 2. Optimal pump switching and corresponding intermediate reservoir water levels.

high water level in the main dam in order to optimise the performance index of the hydropower plant. The top row graphs in Fig. 2 shows the power demand of each of the two pumps, which is 4.82 MW whenever in operation, otherwise it is zero. As shown, the OC switches on K1 to raise the water level of the intermediate reservoir to 50.0 m before bringing in K2 for outward pumping to the main dam. The reservoir water level would fall below its minimum level at 13:00 if pump K2 was operated before K1. The water level drops to the minimum level of 10.0 m at the end of the day. The second row graph shows; the change in water level of the intermediate reservoir as a result of the pumping actions of pumps K1, H_{K1}, and pump K2, H_{K2}. Res_{opt} (m) is the optimal change in the intermediate reservoir water level due to the combined pumping actions of the two pumps. The water level due to the pumping action of K1, H_{K1}, rises steadily to 50.0 m by 11:00. During this period, the overall water level, Res_{opt}, is equal to H_{K1} because pump K2 is off. However, as the OC switches on pump K2 after 11:00, the water level in the intermediate reservoir drops as depicted by H_{k2}. At the end of the control horizon, the intermediate reservoir water level falls to a minimum of 10.0 m, proving that the OC meets all the operational constraints of the model. In addition, the OC scheduling strategy is observed to alternate the pump's operation time in order to minimise the pumping energy. This is one of the main advantages of the cascaded pumpback model over the classical single pump PS model which often consumes a huge amount of energy due to the pump's net hydraulic head for a classical scenario.

4.2. Optimal water level and flow rates of the main dam

The optimal flow rates and the corresponding change in water level of the main dam are shown in Fig. 3. In the figure Q_o and Q_{inflow} are respectively, the turbine flow rate for hydropower generation and the combined in-stream discharge and flow rate of pump K2, $Q_{in} + Q_2$. As shown, Q_{inflow} is 12.50 m^3/s whenever K2 is in off mode and 18.00 m^3/s whenever K2 is in operation mode. The turbine flow rate, Q_o, varies in response to the changes in hydropower load demand, P_g. In this case, Q_o is 24.45 m^3/s between 00:00 and 00:15 but decreases to 22.57 m^3/s between 00:15 and 00:30 in response to a decrease in P_g as shown in Fig. 4. An increase in P_g between 00:30 and 01:00 results in a corresponding increase in Q_o. Between 01:00 and 04:00, Q_o is kept constant at 20.90 m^3/s. However, an increase in P_g from 28.37 MW to 38.37 MW at 04:00 results in a corresponding increase in Q_o from 20.90 m^3/s to 28.27 m^3/s. The optimal water level in the dam, H_{opt} (m), is as a result of the change due to the combined inflows, H_{inflow} (m), less the change due to turbine discharge, H_{Qo} (m). The baseline case is depicted by H_{Qo} which is the would be change in the water level of the dam in the absence of the proposed pumpback system. As shown in Fig. 3, H_{opt} drops from the initial level of 176.00 m to 117.10 m at the end of the day. For the baseline case, the water level in the dam model, H_{Qo}, would drop from 176.00 m to 101.90 m. However, the pumpback system maintains a high water level in the dam to optimise the performance of the plant throughout the control horizon. H_{inflow} shows the would be water level in the dam model if there was inflows without turbine discharge, Q_o. In this case, the water level of the dam model would rise from 176.00 m to 257.30 m, leading to an overflow at the end of the day since the maximum operation level of the dam model is 177.50 m.

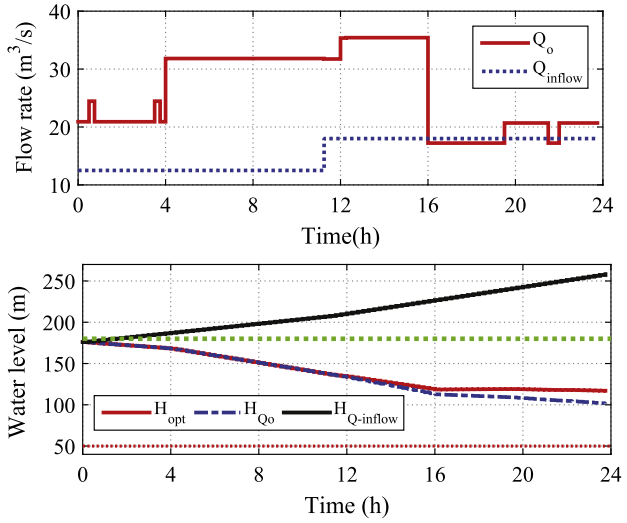

Fig. 3. Flow rates and changes in water level of the main dam in dry season.

4.3. Optimal power flows of the system

Fig. 4 is the optimal power flow of the system based on the measured values for the case of $w_1 = w_2 = w_3 = w_4 = 0.25$. As shown in Fig. 4, the OC uses HK power, P_{hk}, to meet the pumping power demand between 04:00 and 16:00. Afterwards, P_{hk} is zero between 16:00 and 19:30 and between 21:00 and 22:00. This can be attributed to the lower grid load demand hence the grid power, P_{gk}, while much of the produced HK power, P_{hg}, is fed into the grid to conserve water in the main dam. The total pumping energy imported from the grid in the case study is 35.74 MW h.

As shown as well in Fig. 4, all the on-site generated HK power of 21.62 MW is exported to the grid between 00:00 and 00:15, between 00:45 and 03:30, between 16:00 and 19:30 and between 21:30 and 22:00 as the OC opts to meet the pumping power demand by grid import power, P_{gk}. On the other hand, P_g varies in response to changes in grid load supplemented by P_{hg}. For instance, P_g supplies 28.38 MW supplemented by P_{hg} of 21.62 MW to meet the committed demand of 50.00 MW between 00:00 and 00:15. However, a decrease in P_{hg} from 21.62 MW to 16.80 MW at 00:15 against a constant P_{ld} of 50.00 MW results in a corresponding increase in P_g from 28.38 MW to 33.20 MW. This inverse complementary relationship between P_g and P_{hg}, especially between 16:00 and 24:00, is one of the advantages of the proposed optimal control model. A decrease in P_g in response to an increase in P_{hg} conserves water in the dam and optimises the energy output of the dam.

4.4. Uncertainty analysis on optimal power flows

Visual inspection of Fig. 5 of true value power flows shows a close match of the power flows from the measured values, shown in Fig. 4. However, there are some observable differences in pumping power demand between the two cases. When true values are used as shown in Fig. 4, the OC opts to meet the pumping power demand using grid power,P_{gk}, between 01:00 and 08:15 before reverting to HK power, P_{hk}, between 08:15 and 24:00.

The net effect between the two cases is a slight difference in daily grid pumping energy, E_{gk}. The case based on true values results in E_{gk} value of 35.60 MW h as compared to the measured value of 35.74 MW h.

4.5. Optimal daily energy production in dry season

Table 6 shows the optimal energy flows of the proposed model for a typical day in dry season. As shown in the table, weighting factors have effects on the optimal results of the model. In the table, E_K (MW h) denotes the pumping energy demand of the

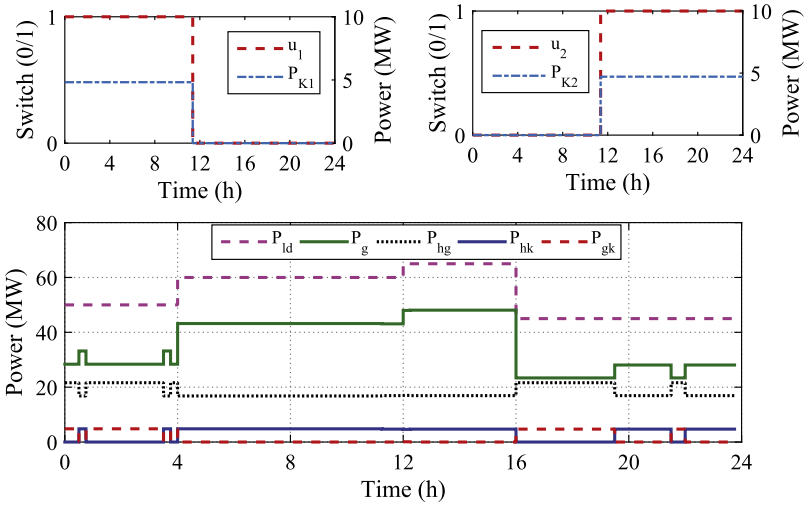

Fig. 4. Optimal power flows of the system in dry season.

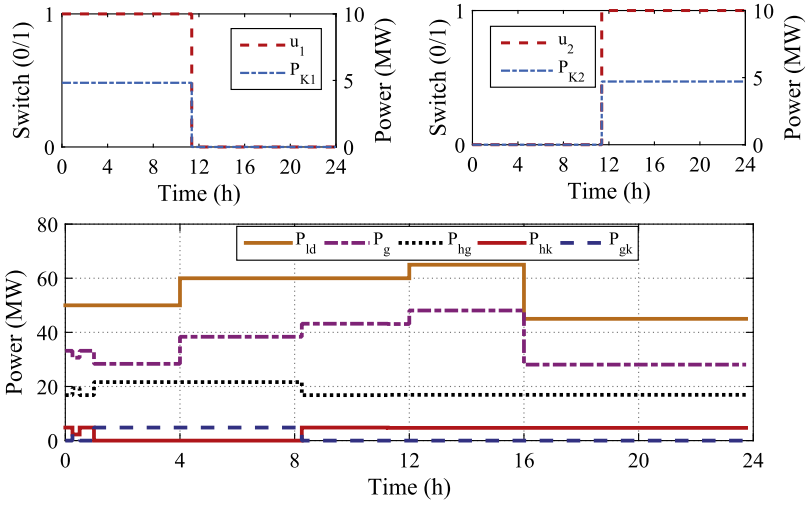

Fig. 5. Sensitivity on the optimal power flows of the cascaded model in dry season.

Table 6
Daily optimal energy flows for a cascaded model in dry season.

$\sum_{i=1}^{4} w_i = 1$	E_g (MW h)	E_{hg} (MW h)	E_{hk} (MW h)	E_{gk} (MW h)	E_K (MW h)	E_{opt} (MW h)	Increase (%)
$w_1 = w_2 = w_3 = w_4 = 0.25$	859.57	440.29	78.69	35.60	114.30	1264.30	47.09
$w_2 = w_3 = w_4 = 0; w_1 = 1$	859.57	440.29	79.36	34.94	114.30	1264.92	47.16
$w_1 = w_3 = w_4 = 0; w_2 = 1$	816.16	518.99	0.00	114.98	114.98	1184.90	45.18
$w_1 = w_2 = w_4 = 0; w_3 = 1$	781.12	518.99	0.00	220.59	220.59	1078.30	38.05
$w_1 = w_2 = w_3 = 0; w_4 = 1$	943.00	356.30	162.68	57.91	220.59	1241.39	31.64

model which is the summation of HK pumping energy, E_{hk} (MW h), and grid pumping energy,E_{gk} (MW h), over the 24 h control horizon. The optimal energy output, E_{opt} (MW h), is the result of summation of hydro-turbine energy output, E_g, excess HK energy supplied to the grid load, E_{hg}, less the grid pumping energy demand, E_{gk}. From Table 6, the objective function simulated using measured values for the case when $w_1 = w_2 = w_3 = w_4 = 0.25$ results in an optimal hydro-turbine energy output, $E_g = \sum P_g t_s = 859.5723$ MW h, where $P_g = g\rho Ho\eta_m\eta_e 10^{-6} Q_o$. In this paper, weighting factors are not optimised, therefore, to ascertain their effects, different combinations of weights are considered. An equal weight to each of the four objective vectors results in grid pumping energy, E_{gk}, of 35.60 MW h and E_{opt} of 1264.30 MW h per day, which translates to 47.09% increase in the daily energy yield of the resultant system.

On the other hand, allocating full priority to minimisation of grid pumping energy, E_{gk}, by setting $w_1 = 1; w_2 = w_3 = w_4 = 0$, results in the best optimal solution with lowest grid pumping energy demand, E_{gk}, of 34.94 MW h which also results in the lowest overall pumping energy demand of 114.30 MW h. This operation strategy increases the overall energy yield of the resultant system by 47.16%, which is the highest gain when compared to other operation strategies. On the other hand, setting $w_1 = w_2 = w_4 = 0; w_3 = 1$, which maximises the restoration of the water level in the main dam by the pumping action of pump K2 results in the highest grid pumping energy demand of

220.59 MW h and 38.05% increase in the overall energy output of the system. This is expected because maximisation of restoration of the volume of the dam results in continuous pumping operation by both pumps K1 and K2 throughout the 24 h control horizon resulting in the highest pumping energy demand of 220.59 with the OC opting to meet it fully by E_{gk}.

The case of setting $w_1 = w_2 = w_3 = 0, w_4 = 1$ results in the optimal solution with the lowest E_{hg} of 356.30 MW h with 31.64% gain in the energy yield of the resultant system, which is the lowest value when compared to other combinations of weighting factors. This is because maximisation of E_{hk} for pumping operation minimises E_{hg} resulting in low gain in E_{opt} despite high E_g. These results with ranging values of weights provide a framework of reference for decision makers when faced with multiple objectives so that effective trade-offs and choices are made with regard to the priority of each of the sub-objectives.

Finally, this proposed model yields results with uncertainty error in the performance index based on true values discussed in sub Sections 3.3.5 and 4.4 equal to:$E_g = \sum P_g t_s = 859.5684$ MW h against the energy output simulated from the measured values of 859.5723 MW h, which are in close agreement. This proves a low risk of uncertainty implying that the model's results have high confidence level to the margin of:

$$\triangle E = \sum P_g t_s \times 0.022 \times 10^{-2} = 0.1891, \tag{36}$$

where 0.022×10^{-2} is the weakest link. A value of $\triangle E = 0.1891$ gives this model the energy output results with the marginal uncertainty error of $E = (859.5723 \pm 0.1891)$.

5. Comparison with the classical single pump pumpback model

The pumpback system for the classical pumped storage (PS) model comprise of a single high lift pump for recycling a part of the down-stream discharge back to the main dam. Fig. 6 shows optimal switching, flow rates and power flows of the classical PS model when $w_1 = w_2 = w_3 = w_4 = 0.25$. As shown, for the same initial conditions of the dam and grid load demand, the OC keeps pump K on throughout the control horizon to maintain the same level of system performance achieved by the cascaded pumpback model. The pumping power demand is 9.19 MW throughout the control period, which is met by P_{gk} between 00:00 and 05:30 and between 19:45 and 20:30, otherwise it is met by P_{hk}.

Table 7 shows energy flows of the classical single pump pumpback model for the same weighting factors used to simulate the results of the cascaded model shown in Table 6. As shown, for the same weighting factors, the pumping energy demand for the classical PS model is far higher for the first three operation strategies as compared to the cascaded pumping model. For instance, for the case when $w_1 = w_2 = w_3 = w_4 = 0.25$, the classical PS model demands an overall pumping energy, E_K, of 220.59 MW h as compared to 114.30 MW h demanded by the cascaded pumpback model.

In this regard, using the classical PS model as the baseline, the cascaded pumpback model saves 106.29 MW h of pumping energy, which translates to a saving of 48.18%. Similarly, the case of $w_1 = 1; w_2 = w_3 = w_4 = 0$ which allocates full optimisation priority to minimisation of grid pumping energy demand results in 114.30 MW h of pumping energy demand for the cascaded model as compared to 219.94 MW h demanded by the single pump classical model. This translates to 48.03% savings in energy demand when the classical PS model is used as the baseline. In similar veins, allocation of full optimisation priority to the restoration of the dam water level by setting $w_1 = w_2 = w_4 = 0; w_3 = 1$, results in an optimal solution with pumping energy demand of 220.59 MW h for both models for the same weighting factors. This is because this operation strategy results in the OC switching on all the pumps throughout the control period in both models resulting in the highest possible pumping energy demand. In comparison, the use of a cascaded pumping model for this case results in 38.05% increase in energy yield of the cascaded model as compared to 24.43% gain realised by the classical PS model. This underscores that the cascaded model has a comparative advantage over the classical PS model even under worst operational strategies.

In general, the high pumping energy demand for the classical single pump PS model as compared to the cascaded pumpback model in the first three operational strategies shown in Tables 6 and 7 is due to the high pumping head bridged by a single pump for the classical model. Optimal operation of the cascaded pumpback system reduces the pumping power and pumping energy demand by alternating the operating schedule of the two pumps at some point over the control horizon as shown in Fig. 2 resulting in lower daily pumping energy.

Scenario II

This is a case of a typical day in the rainy season with high river discharge. Under this scenario, the OC should avoid pumping back water since the river inflows are sufficient to optimally meet the grid power demand.

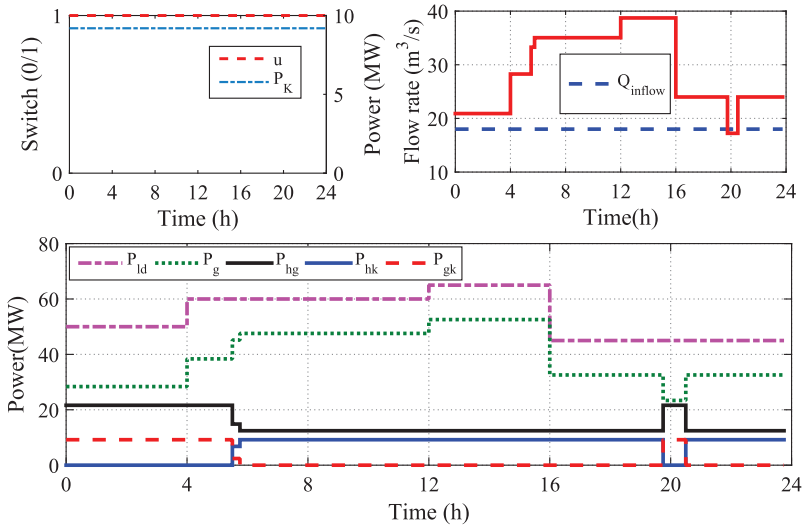

Fig. 6. System power balance of the classical PS model in dry season.

Table 7
Daily optimal energy flows for a classical PS in dry season.

$\sum_{i=1}^{4} w_i = 1$	E_g (MW h)	E_{hg} (MW h)	E_{hk} (MW h)	E_{gk} (MW h)	E_K (MW h)	E_{opt} (MW h)	Increase (%)
$w_1 = w_2 = w_3 = w_4 = 0.25$	943.56	356.44	162.54	58.05	220.59	1242.00	31.63
$w_2 = w_3 = w_4 = 0; w_1 = 1$	908.63	299.05	219.94	0.00	219.94	1207.68	32.91
$w_1 = w_3 = w_4 = 0; w_2 = 1$	873.92	325.79	173.20	47.28	220.48	1152.43	31.87
$w_1 = w_2 = w_4 = 0, w_3 = 1$	867.51	432.49	0.00	220.59	220.59	1079.40	24.43
$w_1 = w_2 = w_3 = 0; w_4 = 1$	943.56	356.44	162.54	58.05	220.59	1242.00	31.63

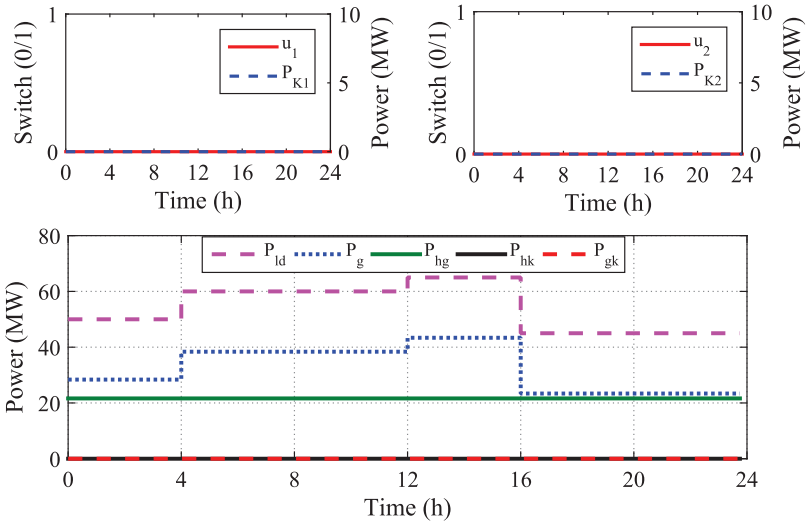

Fig. 7. Optimal power balance of the system in rainy season.

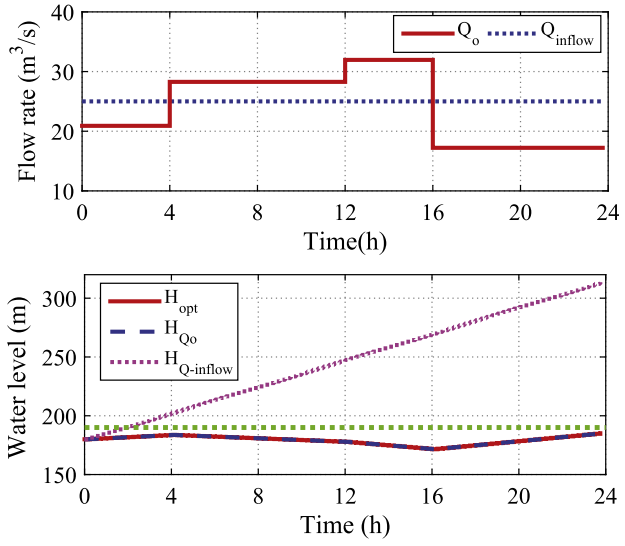

Fig. 8. Optimal flow rates and change in water level of the dam in rainy season.

5.1. Optimal flow rates of the main dam in rainy season

During rain season, Pangani river discharge increases to an average of 25 m^3/s, which is high enough to cover the committed load demand of the power plant. Fig. 7 shows the optimal power flows for the cascaded pumpback model on a typical day in the rainy season. As shown, the OC keeps all the pumps K1 and K2 in off mode and as a result, all the 518.99 MW h of on-site generated HK energy is exported to the grid. Fig. 8 shows the optimal flow rates and the corresponding change in water level of the dam throughout the control period. The constant supply of 21.62 MW of HK power results in low demand for P_g between 16:00 and 24:00 and as a results, a sharp decrease in Q_o from 31.95 m^3/s to 17.22 m^3/s is observed.

Because of the high in-stream flow of 25.0 m^3/s as compared to Q_o of 17.22 m^3/s, the water level of the dam model rises from 171.90 m, to 184.70 m between 16:00 and 24:00 as shown in Fig. 8 resulting in an increase in the water level of the dam.

Table 8 shows the optimal energy flows of the proposed model for a typical day in the rainy season for the case of $w_1 = w_2 = w_3 = w_4 = 0.25$ for both the cascaded and single pump classical model. E_K is zero because the OC opts to operate the pumping system only during dry seasons when there is low in-stream flows and low water levels in the dam. All the on-site generated HK energy of 518.99 MW h is exported to the grid resulting in 66.45% increase in the overall energy yield of the model.

Table 8
Daily optimal energy flows in the rainy season.

$\sum_{i=1}^{4} w_i = 1$	E_g (MW h)	E_{hg} (MW h)	E_{hk} (MW h)	E_{gk} (MW h)	E_K (MW h)	E_{opt} (MW h)	Increase (%)
$w_1 = w_2 = w_3 = w_4 = 0.25$	781.02	518.99	0.00	0.00	0.00	1300.00	66.45

6. Conclusions

Pumpback operation between the afterbay and the main dam to maintain a high water level in the dam can increase the energy output of a hydropower plant in dry season with low in-stream flows. However, the high pumping energy demand associated with high head high flow pumping can derail the economic viability of pumping operation. A cascaded pumping model has the potential to reduce the pumping head and, through optimal operation scheduling, reduce the pumping power and pumping energy demand of the pumpback system. An optimal control for a hydropower plant retrofitted with a hydrokinetic powered pumpback system has been presented in the paper. The objective of the proposed model is to maximise the energy yield of the plant by simultaneously minimising grid pumping energy demand, minimising the wear and tear of the pumps by minimising their switching frequencies, maximising the use of the on-site generated hydrokinetic energy for pumping operation and maximising the restoration of the volume of the dam through pumpback operation. Simulation results based on a practical case study shows the potential of the proposed cascaded pumping model to reduce up to 48.18% of the pumping energy demand and increase the overall energy yield of the resultant system by 30–48% in dry season and up to 66.45% in the rainy season. The high increase in energy yield of the hydropower plant in the later case is due to the exportation of all the on-site generated hydrokinetic energy to the grid in the absence of the pumping operation. When compared to the single pump classical pumpback model, the cascaded pumpback system shows superior performance with lower pumping energy demand. For the case of allocating equal weighting factors to all the four objective vectors, a cascaded pumping model results in an overall pumping energy demand of 114.30 MW h as compared to a high value of 220.59.68 MW h demanded by the classical single pump model. Using the classical model as the operation baseline, the use of a cascaded pumping model results in an energy saving potential of up to 48.18%. For the cascaded pumpback model, the scheduling is observed to alternate the operation of pumps K1 and K2 over the control horizon in order to reduce the overall maximum power demand of the pumps which is one of the main advantages of the cascaded pumping model.

Acknowledgements

The authors would like to thank the MasterCard Foundation, the National Hub for Energy Efficiency and Demand Side Management-South Africa and the University of Zambia-Zambia for financial and other support towards this research.

Appendix A

A.1. Equality matrices

Eq. (17) constitute a sparse matrix $\mathbf{A_{eq1}}$, given in Eq. (A.1) and vector $\mathbf{b_{eq1}}$ shown in Eq. (A.2):

$$\mathbf{A_{eq1}} = \begin{bmatrix} 0 \cdots 0 & 0 \cdots 0 & 0 \cdots 0 & g\rho\eta_e H_o 10^{-6} \cdots 0 & 0 \cdots 0 & 0 \cdots 0 & 1 \cdots 0 & 0 \cdots 0 & 0 \cdots 0 \\ \vdots \ddots \vdots & \vdots \ddots \vdots & \vdots \ddots \vdots & \vdots \ddots \vdots & \vdots \ddots \vdots & \vdots \ddots \vdots & \vdots \ddots \vdots & \vdots \ddots \vdots & \vdots \ddots \vdots \\ 0 \cdots 0_{3N} & 0 \cdots 0 & 0 \cdots 0 & 0 \cdots g\rho\eta_e H_o 10^{-6} & 0 \cdots 0 & 0 \cdots 0 & 0 \cdots 1 & 0 \cdots 0 & 0 \cdots 0 \end{bmatrix}_{N\times 9N} \tag{A.1}$$

$$\mathbf{b_{eq1}} = \begin{bmatrix} P_{ld,1} \\ \vdots \\ P_{ld,N} \end{bmatrix}_{N\times 1}. \tag{A.2}$$

Similarly, the matrix $\mathbf{A_{eq2}}$ shown in Eq. (A.3) and vector $\mathbf{b_{eq3}}$ shown in Eq. (A.4) are constituted from equality constraint (19) for the pump power balance.

$$\mathbf{A_{eq2}} = \begin{bmatrix} -P_{K1} \cdots 0 & -P_{K2} \cdots 0 & 0 \cdots 0 & 0 \cdots 0 & 1 \cdots 0 & 1 \cdots 0 & 0 \cdots 0 & 0 \cdots 0 & 0 \cdots 0 \\ \vdots \ddots \vdots & \vdots \ddots \vdots & \vdots \ddots \vdots & \vdots \ddots \vdots & \vdots \ddots \vdots & \vdots \ddots \vdots & \vdots \ddots \vdots & \vdots \ddots \vdots & \vdots \ddots \vdots \\ 0 \cdots -P_{K1} & 0 \cdots -P_{K2} & 0 \cdots 0 & 0 \cdots 0 & 0 \cdots 1 & 0 \cdots 1 & 0 \cdots 0 & 0 \cdots 0 & 0 \cdots 0 \end{bmatrix}_{N\times 9N} \tag{A.3}$$

$$\mathbf{b_{eq2}} = \begin{bmatrix} 0_1 \\ \vdots \\ 0_N \end{bmatrix}_{N\times 1}. \tag{A.4}$$

Lastly, the matrix $\mathbf{A_{eq3}}$ shown in Eq. (A.5) and vector $\mathbf{b_{eq3}}$ shown in Eq. (A.6) are constituted from the HK power balance of Eq. (18).

$$\mathbf{A_{eq3}} = \begin{bmatrix} 0 \cdots 0 & 0 \cdots 0 & P_h \cdots 0 & 0 \cdots 0 & -1 \cdots 0 & 0 \cdots 0 & -1 \cdots 0 & 0 \cdots 0 & 0 \cdots 0 \\ \vdots \ddots \vdots & \vdots \ddots \vdots & \vdots \ddots \vdots & \vdots \ddots \vdots & \vdots \ddots \vdots & \vdots \ddots \vdots & \vdots \ddots \vdots & \vdots \ddots \vdots & \vdots \ddots \vdots \\ 0 \cdots 0 & 0 \cdots 0 & 0 \cdots P_h & 0 \cdots 0 & 0 \cdots -1 & 0 \cdots 0 & 0 \cdots -1 & 0 \cdots 0 & 0 \cdots 0 \end{bmatrix}_{N\times 9N} \tag{A.5}$$

$$\mathbf{b_{eq3}} = \begin{bmatrix} 0_1 \\ \vdots \\ 0_N \end{bmatrix}_{N\times 1}. \tag{A.6}$$

The canonical form, $\mathbf{A_{eq}X} = \mathbf{b_{eq}}$ is given in Eq. (A.7).

$$\mathbf{A_{eq}} = \begin{bmatrix} \mathbf{A_{eq1}} \\ \mathbf{A_{eq2}} \\ \mathbf{A_{eq3}} \end{bmatrix}_{3N\times 7N}, \qquad \mathbf{b_{eq}} = \begin{bmatrix} \mathbf{b_{eq1}} \\ \mathbf{b_{eq2}} \\ \mathbf{b_{eq3}} \end{bmatrix}_{3N\times 1}, \tag{A.7}$$

A.2. Inequality matrices

The general formulation of the inequality constraint is shown in Eq. (A.8):

$$\mathbf{AX} \leqslant \mathbf{b}. \tag{A.8}$$

Expression (15) constitute the upper boundary matrix $\mathbf{A_1}$ given by Eq. (A.9) and the upper boundary vector $\mathbf{b_1}$ given by Eq. (A.10). Where the lower boundary matrix $\mathbf{A_2} = -\mathbf{A_1}$ and the lower boundary vector $\mathbf{b_2}$ is given by Eq. (A.11).

$$\mathbf{A_1} = \begin{bmatrix} 0 & \cdots & 0 & \frac{Q_2 t_s}{A_u} & \cdots & 0 & 0 & \cdots & 0 & -\frac{t_s}{A_u} & \cdots & 0 & 0 & \cdots & 0 & 0 & \cdots & 0 & 0 & \cdots & 0 & 0 & \cdots & 0 & 0 & \cdots & 0 \\ \vdots & \ddots & \vdots & \vdots & \ddots & \vdots & \vdots & \ddots & \vdots & \vdots & \ddots & \vdots & \vdots & \ddots & \vdots & \vdots & \ddots & \vdots & \vdots & \ddots & \vdots & \vdots & \ddots & \vdots & \vdots & \ddots & \vdots \\ 0 & \cdots & 0 & \frac{Q_2 t_s}{A_u} & \cdots & \frac{Q_2 t_s}{A_u} & 0 & \cdots & 0 & -\frac{t_s}{A_u} & \cdots & -\frac{t_s}{A_u} & 0 & \cdots & 0 & 0 & \cdots & 0 & 0 & \cdots & 0 & 0 & \cdots & 0 & 0 & \cdots & 0 \end{bmatrix}_{N\times 9N}, \tag{A.9}$$

$$\mathbf{b_1} = \begin{bmatrix} h_u^{max} - h_{u,0} - \frac{Q_{in} t_{s,1}}{A_u} \\ \vdots \\ h_u^{max} - h_{u,0} - \frac{Q_{in} t_{s,N}}{A_u} \end{bmatrix}_{N\times 1}, \tag{A.10}$$

$$\mathbf{b_2} = \begin{bmatrix} -h_u^{min} + h_{u,0} + \frac{Q_{in} t_{s,1}}{A_u} \\ \vdots \\ -h_{umin} + h_{u,0} + \frac{Q_{in} t_{s,N}}{A_u} \end{bmatrix}_{N\times 1}. \tag{A.11}$$

Similarly, the inequality constraint (16) constitute the matrix $\mathbf{A_3}$ given by Eq. (A.12) and vector $\mathbf{b_3}$ expressed by Eq. (A.13):

$$\mathbf{A_3} = \begin{bmatrix} \frac{Q_1 t_s}{A_r} & \cdots & 0 & \frac{-Q_2 t_s}{A_r} & \cdots & 0 & 0 & \cdots & 0 & 0 & \cdots & 0 & 0 & \cdots & 0 & 0 & \cdots & 0 & 0 & \cdots & 0 & 0 & \cdots & 0 & 0 & \cdots & 0 \\ \vdots & \ddots & \vdots & \vdots & \ddots & \vdots & \vdots & \ddots & \vdots & \vdots & \ddots & \vdots & \vdots & \ddots & \vdots & \vdots & \ddots & \vdots & \vdots & \ddots & \vdots & \vdots & \ddots & \vdots & \vdots & \ddots & \vdots \\ \frac{Q_1 t_s}{A_r} & \cdots & \frac{Q_1 t_s}{A_r} & \frac{-Q_2 t_s}{A_r} & \cdots & \frac{-Q_2 t_s}{A_r} & 0 & \cdots & 0 & 0 & \cdots & 0 & 0 & \cdots & 0 & 0 & \cdots & 0 & 0 & \cdots & 0 & 0 & \cdots & 0 & 0 & \cdots & 0 \end{bmatrix}_{N\times 9N}, \tag{A.12}$$

$$\mathbf{b_3} = \begin{bmatrix} h_r^{max} - h_{r,0} \\ \vdots \\ h_r^{max} - h_{r,0} \end{bmatrix}_{N\times 1}. \tag{A.13}$$

The lower boundary matrix of the intermediate reservoir $\mathbf{A_4} = -\mathbf{A_3}$ and lower limit vector $\mathbf{b_4}$ is given by Eq. (A.14).

$$\mathbf{b_4} = \begin{bmatrix} -h_r^{min} + h_{r,0} \\ \vdots \\ -h_r^{min} + h_{r,0} \end{bmatrix}_{N\times 1}. \tag{A.14}$$

By letting

$$A_{51} = \begin{bmatrix} 1 & 0 & 0 & \ldots & 0 \\ -1 & 1 & 0 & \ldots & 0 \\ 0 & -1 & 1 & \ldots & 0 \\ \vdots & \vdots & \ddots & \ddots & \vdots \\ 0 & 0 & \ldots & -1 & 1 \end{bmatrix}_{N\times N}, \qquad A_{52} = \begin{bmatrix} -1 & 0 & 0 & \ldots & 0 \\ 0 & -1 & 0 & \ldots & 0 \\ 0 & 0 & -1 & \ldots & 0 \\ \vdots & \vdots & \vdots & \ddots & \vdots \\ 0 & 0 & 0 & \ldots & -1 \end{bmatrix}_{N\times N} \tag{A.15}$$

then, inequality (25) can be written as

$$A_5 = [A_{51} \quad A_{51} \quad (0 \ldots 0)_{5N} \quad A_{52} \quad A_{52}]_{N \times 9N}$$
$$b_5 = [0 \quad 0 \quad 0 \quad \ldots \quad 0]^T_{N \times 1} \tag{A.16}$$

Thus, the final expression of the matrix **A** and vector **b** is given by Eq. (A.17)

$$\mathbf{A} = \begin{bmatrix} \mathbf{A_1} \\ \mathbf{A_2} \\ \mathbf{A_3} \\ \mathbf{A_4} \\ \mathbf{A_5} \end{bmatrix}_{5N \times 9N}, \qquad \mathbf{b} = \begin{bmatrix} \mathbf{b_1} \\ \mathbf{b_2} \\ \mathbf{b_3} \\ \mathbf{b_4} \\ \mathbf{b_5} \end{bmatrix}_{5N \times 1}. \tag{A.17}$$

References

[1] van Vliet MT, Wiberg D, Leduc S, Riahi K. Power-generation system vulnerability and adaptation to changes in climate and water resources. Nature Climate Change 2016;6:375–80.
[2] R. Beilfuss, A risky climate for southern african hydro, International Rivers, Berkely.
[3] Harrison GP, Whittington H. Vulnerability of hydropower projects to climate change. IEE proceedings-generation, transmission and distribution, vol. 149. IET; 2002. p. 249–55.
[4] Yeh WW-G. Reservoir management and operations models: a state-of-the-art review. Water Resources Res 1985;21(12):1797–818.
[5] Labadie JW. Optimal operation of multireservoir systems: state-of-the-art review. J Water Resources Plan Manage 2004;130(2):93–111.
[6] Jacovkis PM, Gradowczyk H, Freisztav AM, Tabak EG. A linear programming approach to water-resources optimization. Zeitschrift für Oper Res 1989;33 (5):341–62.
[7] Edwards BK, Flaim SJ, Howitt RE. Optimal provision of hydroelectric power under environmental and regulatory constraints. Land Econ 1999:267–83.
[8] Gao H, Wang C. A optimal operation scheduling method of pumped storage station and thermal power station coordination. In: 2006 IEEE PES power systems conference and exposition. IEEE; 2006. p. 1829–32.
[9] Liang R-H. A noise annealing neural network for hydroelectric generation scheduling with pumped-storage units. IEEE Trans Power Syst 2000;15 (3):1008–13.
[10] Pritchard G, Philpott AB, Neame PJ. Hydroelectric reservoir optimization in a pool market. Math Programming 2005;103(3):445–61.
[11] Yoo J-H. Maximization of hydropower generation through the application of a linear programming model. J Hydrol 2009;376(1):182–7.
[12] Loisel R, Mercier A, Gatzen C, Elms N, Petric H. Valuation framework for large scale electricity storage in a case with wind curtailment. Energy Policy 2010;38(11):7323–37.
[13] Lu N, Chow JH, Desrochers AA. Pumped-storage hydro-turbine bidding strategies in a competitive electricity market. IEEE Trans Power Syst 2004;19 (2):834–41.
[14] Cohen AI, Wan S. An algorithm for scheduling a large pumped storage plant. IEEE Trans Power Apparatus Syst 1985(8):2099–104.
[15] Guan X, Luh PB, Yen H, Rogan P. Optimization-based scheduling of hydrothermal power systems with pumped-storage units. IEEE Trans Power Syst 1994;9(2):1023–31.
[16] Li W, Huang J, Li G, Wang Z. Research on optimizing operation of the single reservoir of hybrid pumped storage power station. In: 2011 4th International conference on electric utility Deregulation and Restructuring and Power Technologies (DRPT). IEE; 2011. p. 1389–94.
[17] Zhao G, Davison M. Optimal control of hydroelectric facility incorporating pump storage. Renew Energy 2009;34(4):1064–77.
[18] Lansey KE, Awumah K. Optimal pump operations considering pump switches. J Water Resources Plan Manage 1994;120(1):17–35.
[19] Zhuan X, Xia X. Optimal operation scheduling of a pumping station with multiple pumps. Appl Energy 2013;104:250–7.
[20] Tang Y, Zheng G, Zhang S. Optimal control approaches of pumping stations to achieve energy efficiency and load shifting. Int J Electr Power Energy Syst 2014;55:572–80.
[21] Wanjiru EM, Zhang L, Xia X. Model predictive control strategy of energy-water management in urban households. Appl Energy 2016;179:821–31.
[22] Arce A, Ohishi T, Soares S. Optimal dispatch of generating units of the itaipú hydroelectric plant. IEEE Trans Power Syst 2002;17(1):154–8.
[23] Tang Y, Zheng G, Zhang S. Optimal control approaches of pumping stations to achieve energy efficiency and load shifting. Int J Electr Power Energy Syst 2014;55:572–80.
[24] Lago L, Ponta F, Chen L. Advances and trends in hydrokinetic turbine systems. Energy Sustain Dev 2010;14(4):287–96.
[25] Ashok S. Optimised model for community-based hybrid energy system. Renew Energy 2007;32(7):1155–64.
[26] Sichilalu S, Mathaba T, Xia X. Optimal control of a wind–pv–hybrid powered heat pump water heater. Appl Energy 2015. http://dx.doi.org/10.1016/j.apenergy.2015.10.072 [in press], Corrected proof.
[27] Wanjiru EM, Xia X. Energy-water optimization model incorporating rooftop water harvesting for lawn irrigation. Appl Energy 2015;160:521–31.
[28] Kimwaga R, Nkandi S. Evaluation of the suitability of pangani falls redevelopment (hydro power) project in pangani river basin, tanzania: an iwrm approach.
[29] Luteganya K, Kizzy S. Hydroelectric power modelling study. Pangani river basib flow assessment, Print; January 2009.
[30] Sichilalu SM, Xia X. Optimal energy control of grid tied pv–diesel–battery hybrid system powering heat pump water heater. Solar Energy 2015;115:243–54.